4DCT-based measurement of changes in pulmonary function following a course of radiation therapy

Kai Ding
Department of Biomedical Engineering, The University of Iowa, Iowa City, Iowa 52242

John E. Bayouth and John M. Buatti
Department of Radiation Oncology, The University of Iowa, Iowa City, Iowa 52242

Gary E. Christensen
Department of Radiation Oncology, The University of Iowa, Iowa City, Iowa 52242
and Department of Electrical and Computer Engineering, The University of Iowa, Iowa City, Iowa 52242

Joseph M. Reinhardt[a)]
Department of Biomedical Engineering, The University of Iowa, Iowa City, Iowa 52242

(Received 31 July 2009; revised 7 January 2010; accepted for publication 18 January 2010; published 24 February 2010)

Purpose: Radiation therapy (RT) for lung cancer is commonly limited to subtherapeutic doses due to unintended toxicity to normal lung tissue. Reducing the frequency of occurrence and magnitude of normal lung function loss may benefit from treatment plans that incorporate the regional lung and radiation dose information. In this article, the authors propose a method that quantitatively measures the regional changes in lung tissue function following a course of radiation therapy by using 4DCT and image registration techniques.
Methods: 4DCT data sets before and after RT from two subjects are used in this study. Nonlinear 3D image registration is applied to register an image acquired near end inspiration to an image acquired near end expiration to estimate the pulmonary function. The Jacobian of the image registration transformation, indicating local lung expansion or contraction, serves as an index of regional pulmonary function. Approximately 120 annotated vascular bifurcation points are used as landmarks to evaluate registration accuracy. The authors compare regional pulmonary function before and after RT to the planned radiation dose at different locations of the lung.
Results: In all registration pairs, the average landmark distances after registration are on the order of 1 mm. The pulmonary function change as indicated by the Jacobian change ranges from −0.15 to 0.1 in the contralateral lung and −0.22 to 0.23 in the ipsilateral lung for subject A, and ranges from −0.4 to 0.39 in the contralateral lung and −0.25 to 0.5 in the ipsilateral lung for subject B. Both of the subjects show larger range of the increase in the pulmonary function in the ipsilateral lung than the contralateral lung. For lung tissue regions receiving a radiation dose larger than 24 Gy, a decrease in pulmonary function was observed. For regions receiving a radiation dose smaller than 24 Gy, either an increase or a decrease in pulmonary function was observed. The relationship between the pulmonary function change and the radiation dose varies at different locations.
Conclusions: With the use of 4DCT and image registration techniques, the pulmonary function prior to and following a course of radiation therapy can be measured. In the preliminary application of this approach for two subjects, changes in pulmonary function were observed with a weak correlation between the dose and pulmonary function change. In certain sections of the lung, detected locally compromised pulmonary function may have resulted from radiation injury. [DOI: 10.1118/1.3312210]

Key words: image registration, radiation therapy, pulmonary

I. INTRODUCTION

Radiation therapy (RT) for lung cancer is commonly limited to subtherapeutic doses due to unintended toxicity to normal lung tissue. The radiation dose needed to control the tumor is well above that which causes toxicity to the normal lung tissue. Increase in tumor control could be achieved by delivering substantially higher radiation doses to the tumor,[1] which is optimally achieved with RT delivery schemes that reduce toxicity. Reducing the frequency of occurrence and magnitude of normal lung function loss may benefit from treatment plans that incorporate relationships between regional and functional based lung information and the radiation dose.

The complex inter-relationship between RT treatment dose and pulmonary function change/toxicity are poorly defined. Common toxicities include radiation pneumonitis, radiation fibrosis, and, ultimately, altered respiratory capacity. Recent dose escalation studies of radiosurgery show a clear dose response relationship for primary lung tumors and that toxicity increased with dose.[2–5] The relationship between ra-

diation dose and normal lung tissue toxicity has been investigated since CT based planning became commonplace over a decade ago,[6] yet the clear indicators for toxicity remain elusive.[7–11] It has been broadly accepted that radiation dose has a direct effect on treated lung tissue and the lung in the treatment field shows radiographic fibrotic changes consistent with fibrosis.[12] It is largely assumed that this is the predominant and, in some cases, only significant effector of altered lung function despite known changes in inflammatory cells outside the treated area. Most current avoidance methods for lung tissue are solely based on direct dose-volume relationships with treated lung,[6,9,13,14] assuming lung tissue is homogeneous in its response to toxicity, irrespective of tissue location or underlying function.[15] Recently, Yaremko *et al.*[15] proposed a method incorporating image registration derived estimate of ventilation to reduce normal lung irradiation. However, the radiation induced pulmonary function change may depend on the location, underlying function of that lung prior to radiations, radiation dose, and other factors, especially in diseased lungs.[16,17] No human studies have investigated the relationships between local lung function, spatial radiation dose distribution, and radiation induced lung function changes. However, rat studies have investigated changes in pulmonary function based on irradiation of different regions of rat lung. van Luijk *et al.*[18] showed structural changes in the lung were only correlated with changes in breathing rate when irradiating lateral lung regions (shielding the mediastinum), and that greater lung damage was observed when irradiating the heart[19] while holding the mean lung dose and the volume of lung irradiated constant. They showed that irradiation of larger volumes with smaller doses causes greater toxicity than treating smaller volumes with larger doses.[20] This is a result confirmed by others.[21] A common yet unspecified thread in the rat studies is that radiation treatments including the mediastinum caused a greater change in pulmonary function. Establishing a quantitative measurement of the pulmonary function change before and after RT may greatly accelerate similar studies of the relationship between RT treatment and resultant changes in pulmonary function. Furthermore, this could translate into clinically relevant data for future treatment planning schemes that avoid increased functional injury to the lungs.

The pulmonary function test is a common clinical measurement tool to assess lung function, but only provides global information on the entire respiratory system. Regional pulmonary function can be measured using various imaging modalities. Nuclear medicine imaging, such as positron emission tomography and single photon emission CT, can provide an assessment of local lung function.[22–24] Hyperpolarized noble gas MR imaging has been developed for functional imaging of pulmonary ventilation.[25–27] Xenon-enhanced CT (Xe-CT) can measure regional ventilation by observing the gas wash-in and wash-out rate on serial CT images.[28,29] Image registration has been used to assess regional lung function and tissue biomechanics using multiple 3D images at different lung volumes by CT[30–32] and MRI.[33] Image registration derived regional expansion can be used to indicate pulmonary function since there is a high correlation between regional lung expansion and regional ventilation. We previously demonstrated a correlation between the image registration based estimate of regional expansion (average Jacobian) and the Xe-CT derived specific ventilation[32] (linear regression, average $r^2=0.73$) in both static and dynamic image acquisition.[34]

This paper describes a technique using 4DCT, image registration, and lung biomechanical analysis to measure regional lung function before and after radiation therapy. The validity of the nonrigid image registration is evaluated by independently assessing 120 vascular bifurcation points within the lung. Changes in regional lung function before and after RT are compared to the radiation dose distribution by transforming the pulmonary function maps into the same coordinate system as that of the computed dose distribution. This provides a framework to examine the relationship between lung function change, delivered dose, and treatment location within the lung.

II. MATERIAL AND METHODS

II.A. Method overview

Our goal is to measure changes in lung function by comparing regional lung volumes at end inspiration (EI) and end expiration (EE) before and after treatment. Figure 1 shows a block diagram of the entire process. Five image data sets are used in the processing. A "free breathing" pretreatment (FB_{PRE}) fan beam CT scan for treatment planning is acquired prior to RT using an ungated protocol with the subject breathing quietly during the scan. The FB_{PRE} image is used during the treatment planning process as the target data set; all radiation dose calculations and daily localization procedures are registered to the FB_{PRE} CT coordinate system. A 4DCT scan is also acquired prior to RT, and CT data sets are reconstructed at ten distinct phases of respiration. For this study, we focus on the data sets from two of the phases, a volume at end expiration (EE_{PRE}) and a volume at end inspiration (EI_{PRE}). A second 4DCT study was acquired after RT and used in this study as "post" RT scans for analysis of post-RT changes (EE_{POST} and EI_{POST}).

Nonlinear image registration is used to define four transformations on these data sets. Table I summarizes these four transformations. Transformations T1 and T2 are defined between respiratory phase points on the 4DCT, and are used to estimate local lung expansion. Transformations T3 and T4 are used to convert the lung expansion data into same coordinate system as the RT dose map, and are used to compare changes in lung expansion with delivered RT dose.

Local lung function is assessed via the Jacobian (JAC) of the transformations T1 and T2 which register EI to EE data. The Jacobian of the transformation T1 (JAC_{PRE}) describes the volume changes from EI_{PRE} to EE_{PRE} and the Jacobian of transformation T2 (JAC_{POST}) describes the volume changes from EI_{POST} to EE_{POST}. To compare these changes, the Jacobian of T1 and the Jacobian of T2 were mapped to the FB_{PRE} coordinate system with transformations T3 and T4, respectively. Additional details on the registration algorithms and other processing steps are given below.

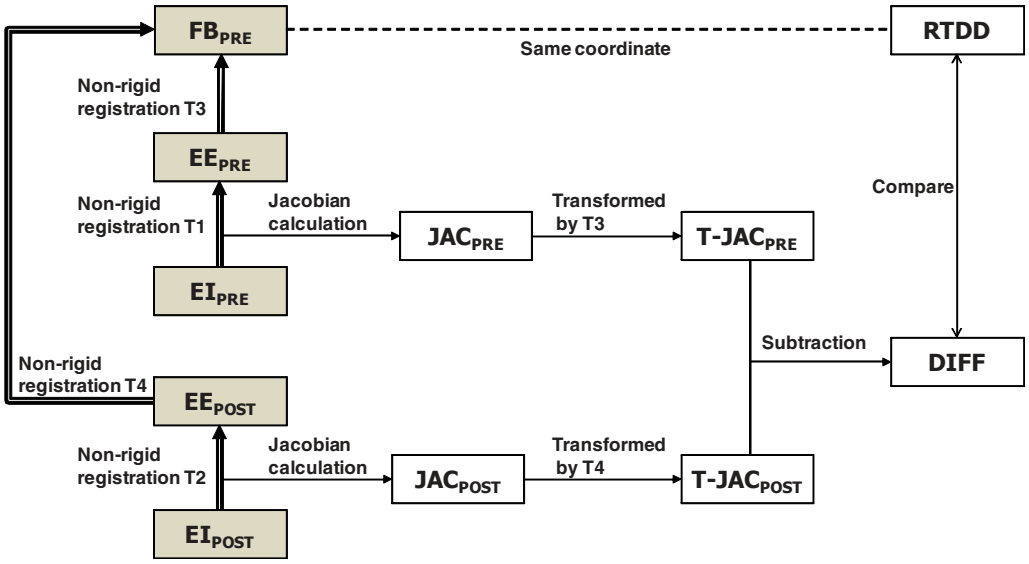

FIG. 1. Figure shows the five images (EE_{PRE}, EI_{PRE}, EE_{POST}, EI_{POST}, and FB_{PRE}) that are analyzed during the processing. Transformations T1 and T2 register EI to EE data and can be used to assess local lung function via the JAC of the transformations. PRE and POST indicate before and after RT. The DIFF between the pretreatment and post-treatment Jacobian data can be used to look for changes in pulmonary function. Transformations T3 and T4 map the Jacobian data into the coordinate system of the FB_{PRE} (planning CT) image, which allows direct comparison with the radiation treatment dose distribution (RTDD). FB_{PRE} and RTDD are in the same coordinate system since the FB_{PRE} scan is used to create the dose plan. (Shaded boxes indicate CT image data; white boxes indicated derived or calculated data; thick arrows indicate image registration transformations being calculated; thin solid lines indicate other operations.)

II.B. Image data sets

All data sets were gathered under a protocol approved by the University of Iowa IRB. Data sets from two subjects with lung tumors treated in the Department of Radiation Oncology at the University of Iowa Hospitals and Clinics were analyzed retrospectively for this study: All scans were acquired as clinically indicated. Both subjects had two 4DCT studies—The first study was prior to the first course of RT and the second study followed delivery of RT. Both 4DCT studies included a contrast-enhanced free breathing CT scan used for RT treatment planning dose calculations. Prior to each 4DCT scan, the subject received respiratory training using a biofeedback system (RESP@RATE, Intercure Ltd., Lod, Israel) to identify their nominal breathing rate. Musical cues were used to pace respiration during imaging, employing a technique developed at our institution and shown to have high success and compliance.[37]

For subject A, the EE_{POST} and EI_{POST} data were acquired after a complete course of RT treatments (approximately 1 yr after the FB_{PRE} scan and 48 Gy in 16 Gy/fx for three fractions). For subject B, the EE_{POST} and EI_{POST} data were acquired after 13 of 37 fractions (23.4 Gy in 1.8 Gy/fx out of 66.6 Gy total), approximately one month later after the FB_{PRE} scan. These patient scans were selected for analysis because they contained 4DCT data sets both pre-RT and post-RT, with a known planned dose distribution. For subject A, the tumor was a solitary mass (~ 4 cm^3) located in the left lung and the right lung was disease-free. For subject B, the tumor was located in the right lung as well as the mediastinum and extending all the way up into the right supraclavicular region, while the left lung was disease-free. Each volumetric data set was acquired with a section spacing of 2–3 mm and a reconstruction matrix of 512×512. In-plane pixel spacing is approximately 0.97×0.97 mm^2.

TABLE I. Summary of image registrations performed to detect RT-induced changes in lung function. Names of images and transformations refer to those given in Fig. 1.

Transformation name	Image transformed	Used to	Algorithm used
T1	$EI_{PRE} \rightarrow EE_{PRE}$	Calculate pre-RT lung expansion map (Jacobian of T1)	SICLE[a]
T2	$EI_{POST} \rightarrow EE_{POST}$	Calculate post-RT lung expansion map (Jacobian of T2)	SICLE[a]
T3	$EE_{PRE} \rightarrow FB_{PRE}$	Transform pre-RT Jacobian into RT dose planning system coordinate system for comparison	SICLE[a]
T4	$EE_{POST} \rightarrow FB_{PRE}$	Transform post-RT Jacobian into RT dose planning system coordinate system for comparison	ELASTIX-NRP[b]

[a]Reference 35.
[b]Reference 36.

II.C. Image registration

II.C.1. Small deformation inverse consistent linear elastic (SICLE) image registration

SICLE (Ref. 35) was used to estimate transformations T1, T2, and T3 shown in Table I and Fig. 1. The SICLE algorithm minimizes the inverse consistency error between the forward transformation h from template image T to target image S and the reverse transformation g from S to T, providing more accurate correspondences between two images compared to algorithms that independently estimate forward and reverse transformations. The transformations h and g are jointly estimated by minimizing the cost function

$$C = \sigma\left(\int_\Omega |T(h(x)) - S(x)|^2 dx + \int_\Omega |S(g(y)) - T(y)|^2 dy\right) + \chi\left(\int_\Omega \|h(x) - g^{-1}(x)\|^2 dx + \int_\Omega \|g(y) - h^{-1}(y)\|^2 dy\right) + \rho\left(\int_\Omega \|Lu(x)\|^2 dx + \int_\Omega \|Lw(y)\|^2 dy\right), \quad (1)$$

where Ω is the domain of the images T and S. Assume that $h(x)=x+u(x)$, $h^{-1}(y)=y+\tilde{u}(y)$, $g(y)=y+w(y)$, and $g^{-1}(x)=x+\tilde{w}(x)$, where $h^{-1}(h(x))=x$ and $g^{-1}(g(y))=y$. Here u, w, $\tilde{u}$, and $\tilde{w}$ are called displacement fields since they define the transformation in terms of a displacement from a location x. The first two integrals of the cost function define the cumulative intensity squared error (shape differences) between the deformed image $T\circ h$ and image S and the differences between the deformed image $S\circ g$ and image T. The second two integrals define the inverse consistency error which is minimized when $h=g^{-1}$. This constraint couples the estimation of h and g together and penalizes transformations that are not inverses of each other. The third two integrals are linear elastic constraint, which applies the linear elasticity operator[35] L to ensure that the transformations maintain the topology of the images T and S. This term is used to regularize the forward and reverse voxel displacement fields $u(x)$ and $w(y)$, so that they are smooth and continuous by penalizing large derivatives of the displacement fields. For this study, the weighting constants were set as $\sigma=1$, $\chi=600$, and $\rho=0.001\ 25$. These parameters are similar to those used in our previous work.[32]

II.C.2. B-splines image registration with local rigidity penalty (ELASTIX-NRP)

A high probability exists for the tumor to have changed fundamentally in size and shape between the FB_{PRE} study and the EE_{POST} and EI_{POST} scans, since substantial radiation dose has been delivered and significant time has passed. In order to avoid introducing an apparent local function change, due to tumor size change due to RT, the T4 transformation that registers EE_{POST} to FB_{PRE} is computed by a nonrigid registration with a local rigidity penalty (NRP) term[36] using ELASTIX (http://elastix.isi.uu.nl). The EE_{POST} image is registered to the FB_{PRE} image using mutual information and a B-splines parameterized transformation. To define the local rigidity constraint, the lung is segmented using the method from Ref. 38 and the tumor region is manually segmented. The nonrigid registration with local rigidity penalty term method has been previously described in Ref. 36. The impact of the local rigidity penalty was analyzed by visual inspection, difference imaging, and overall quantitative effect on computed vector displacement of voxels within and immediately surrounding the tumor.

II.D. Computational setup

Processing starts by resampling all five CT data sets to a voxel size of $1\times1\times1$ mm^3. After resampling, the main airways are identified on all images using the PULMONARY WORKSTATION 2.0 (VIDA Diagnostics, Inc., Iowa City, IA). The airway segmentation algorithm uses a seeded region growing method with an adaptive threshold. The segmentation is initialized with seed voxels from the trachea. After airway segmentation, the images are translated into a common coordinate system by aligning the carinas. Image FB_{PRE} is defined as the reference image.

After this preprocessing, EE_{PRE} is registered to FB_{PRE} using SICLE to find T3. Next, T1 (EI_{PRE} to EE_{PRE}) and T2 (EI_{POST} to EE_{POST}) are estimated using SICLE.

To find T4 (EE_{POST} to FB_{PRE}), the nonrigid registration with local rigidity penalty term method is applied. This registration is performed in two stages. For the first stage of initial alignment, five image resolutions are used and no lung mask and rigid penalty term are applied. B-spline grid spacing is set to 10 voxels and the number of optimization iterations is 500 for each resolution. For the second stage of fine alignment, the lung mask in the target image (FB_{PRE}) is applied and rigid penalty term is specified. The rigidity is set to 1.0 in the tumor region and 0.0 in other lung regions. In this stage, the full resolution images are registered with B-spline grid spacing of 10 voxels followed by registration using B-spline grid spacing of 5 voxels. In this way, the cost function is first optimized for the whole lung region, and then specifically for the rigid tumor region. For more details about the parameter settings for our study, please see http://elastix.isi.uu.nl/wiki.php.

II.E. Assessment of image registration accuracy

Approximately 120 vascular bifurcation points are used as landmarks to evaluate registration accuracy. A landmark annotating system[39] is used to guide the observer to find the corresponding landmarks in the FB_{PRE}, EE_{PRE}, EI_{PRE}, EE_{POST}, and EI_{POST} images. Each landmark pair manually annotated by the observer was added to a thin-plate spline to warp the FB_{PRE} image and predict the position for the next unmatched landmark for the observer. The matching task for the observer becomes easier as the warped image is deformed by previously selected landmarks. For each landmark, the actual landmark position is compared to the registration derived estimate of landmark position and the landmark error is calculated.

II.F. Computing changes in pulmonary function

Lung volume change across respiratory cycle is predominantly due to inspired or expired air.[40,41] Lung ventilation is defined as the volume of air inspired into or expired out of the lungs in a unit time (usually in 1 min), so air volume change is proportional to ventilation. Therefore, lung volume change should be correlated with ventilation and specific volume change should be correlated with specific ventilation. We previously showed that the Jacobian is directly related to local specific volume change (sVol, expansion) as $\mathrm{sVol}=J-1$, where J is the Jacobian of the image registration transformation between two images acquired at different lung volumes.[32] Thus, the Jacobian should also be correlated with specific ventilation. Using a sheep model, we compared the regional lung expansion estimated by registering images acquired at different pressures (breath-hold) and respiratory phases (tidal breathing) with the xenon CT specific ventilation in four adult sheep. Regional lung expansion, as estimated from the Jacobian of the image registration transformations, was well correlated with xenon CT specific ventilation[32,34] (linear regression, average $r^2=0.73$). Therefore, the Jacobian can be used as a local measure of pulmonary function. Note that the image pairs used to estimate regional pulmonary expansion via the Jacobian must be acquired within a relatively short time interval or the assumption that all lung volume change is due to air volume change may not hold.

In our process, local lung expansion can be calculated from the Jacobian of the transformations T1 and T2. The vector transformation function $h(x)$ that maps image T to image S as described in Section II C is used to calculate the local lung expansion and contraction using the Jacobian determinant $J(h(x))$ defined as

$$J(h(x))=\begin{vmatrix} \frac{\partial h_1(x)}{\partial x_1} & \frac{\partial h_2(x)}{\partial x_1} & \frac{\partial h_3(x)}{\partial x_1} \\ \frac{\partial h_1(x)}{\partial x_2} & \frac{\partial h_2(x)}{\partial x_2} & \frac{\partial h_3(x)}{\partial x_2} \\ \frac{\partial h_1(x)}{\partial x_3} & \frac{\partial h_2(x)}{\partial x_3} & \frac{\partial h_3(x)}{\partial x_3} \end{vmatrix}, \quad (2)$$

where $h_1(x)$ is the x component of $h(x)$, $h_2(x)$ is the y component of $h(x)$, and $h_3(x)$ is the z component of $h(x)$. In a Lagrangian reference frame, there is local tissue expansion if the Jacobian is greater than 1 and there is local tissue contraction if the Jacobian is less than 1. If we consider a small volume V_s at point x in S and the corresponding volume V_t at $h(x)$ in T, then $J(h(x))=V_t/V_s$. Therefore, if a lung tissue point has $J(h(x))=1.5$, it means the $V_t=1.5V_s$. Based on our earlier findings,[32,34] a higher Jacobian value reflects a higher specific ventilation.

Transformations T3 and T4 transform the Jacobian data into the coordinate system of $\mathrm{FB_{PRE}}$, where they can be compared to look for changes in lung function. As shown in Fig. 1, the subtraction of the transformed Jacobian data $\mathrm{T\text{-}JAC_{PRE}}$ from the Jacobian data $\mathrm{T\text{-}JAC_{POST}}$ results in the Jacobian difference image which is the image of the pulmonary function change.

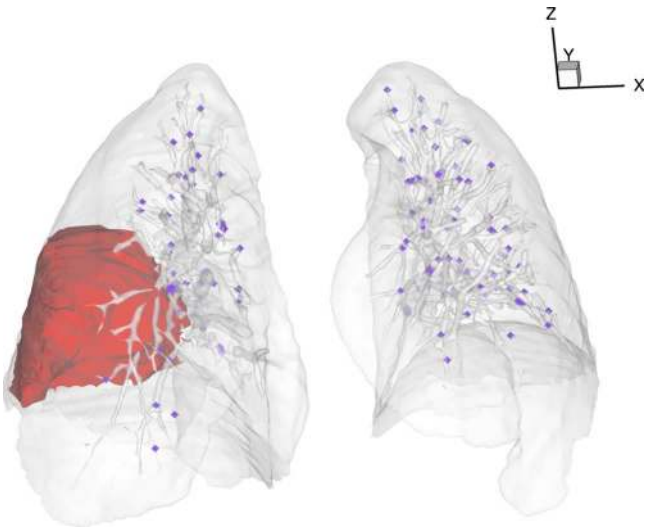

FIG. 2. 3D view of landmarks as vessel bifurcation points in the $\mathrm{FB_{PRE}}$ for subject B. The dark region on the left side of the figure is the manually segmented tumor and the spheres are the manually defined landmarks.

II.G. Comparing regional pulmonary function change to planned radiation dose distribution

We are interested in looking at the resultant change in the local Jacobian and comparing those changes with the computed RT planning system dose distribution map. The radiation dose distribution image has voxel size of $4\times4\times4$ mm^3 (PINNACLE treatment planning system, version 8.0). Linear interpolation was used to resample the radiation dose distribution image to the same voxel size as the $\mathrm{FB_{PRE}}$ image ($1\times1\times1$ mm^3). After interpolation, the Jacobian difference and the dose distribution image were aligned to the $\mathrm{FB_{PRE}}$ image. Registration of both images and the dose distribution to a common coordinate system allows the radiation dose and the change in pulmonary function to be compared.

III. RESULTS

III.A. Registration accuracy

Approximately 120 manually identified landmarks within the lungs were used to compute registration accuracy. The landmarks were nominally uniformly distributed between two lungs for each subject. Figure 2 shows an example of the distribution of the landmarks in subject B for the $\mathrm{FB_{PRE}}$ image, where the red region is the manually segmented tumor within the right lung and the blue spheres are the landmarks. The (x,y,z) coordinate of each landmark location was recorded for each CT data set ($\mathrm{EI_{PRE}}$, $\mathrm{EE_{PRE}}$, $\mathrm{EI_{POST}}$, $\mathrm{EE_{POST}}$, and $\mathrm{FB_{PRE}}$) before and after registration for both subjects. Figure 3(a) shows the magnitude of respiratory motion for subject A prior to RT, with anatomical landmarks having pre-RT excursions of 2–12 mm in the contralateral lung and

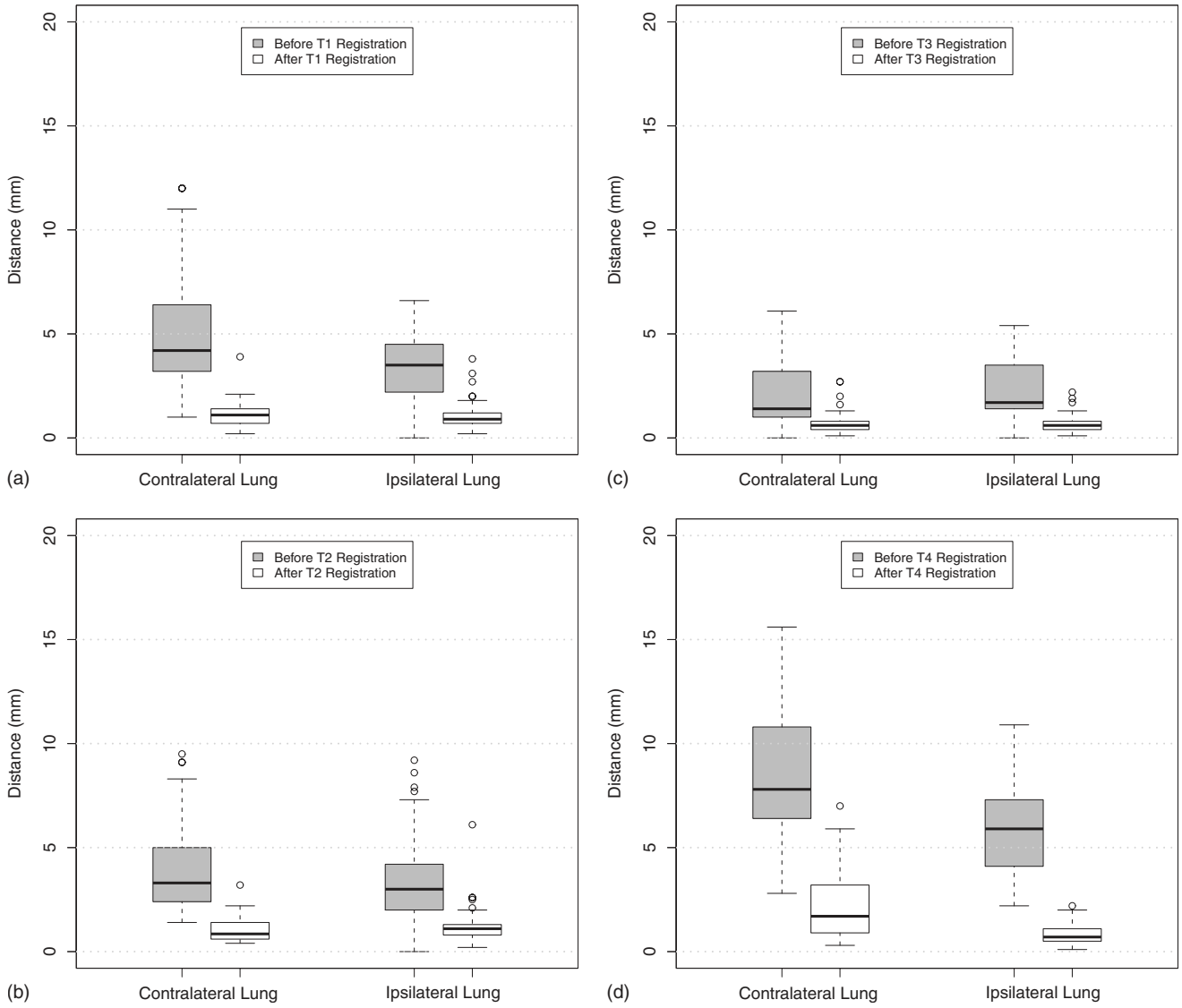

FIG. 3. Landmark distances for subject A before and after registration. Distances between registration pairs (a) T1: EI_{PRE} and EE_{PRE}; (b) T2: EI_{POST} and EE_{POST}; (c) T3: EE_{PRE} and FB_{PRE}; and (d) T4: EE_{POST} and FB_{PRE}. Box plot lower extreme is first quartile; box plot upper extreme is third quartile. Median is shown with solid horizontal line. Whiskers show either the minimum (maximum) value or extend 1.5 times the first to third quartile range beyond the lower (upper) extreme of the box, whichever is smaller (larger). Outliers are marked with circles.

half that distance in the ipsilateral lung. Following the nonrigid registration of the EI_{PRE} and EE_{PRE} data sets, the average landmark distances are of the order of 1 mm. Figure 3(b) shows similar motion of landmarks post-RT before registration, with ~1 mm distances between landmark points following registration. The registration pair EE_{PRE} and FB_{PRE} [Fig. 3(c)] shows the smallest landmark distance both before and after registration in two cases. The amplitude of breathing during the free breathing scan FB_{PRE} was assumed to have been acquired with a mean position predominantly weighted by the end of expiration of 4DCT. Thus, there is little anatomic difference in the registration pair EE_{PRE} and FB_{PRE} compared to other registration pairs. Conversely, Fig. 3(d) shows the EE_{POST} is different from the FB_{PRE} image, as these are acquired on different days. For this subject, the nonrigid registration produced superior agreement between landmarks in the ipsilateral lung than observed in the contralateral lung. The respiratory motion from subject B (Fig. 4) produced larger pre-RT excursions (range 2–18 mm) which were reduced overall following ~23 Gy of RT. Overall, the post-RT excursions [Fig. 4(b)] were of the same magnitude in the both lungs. The trends for subject B in Figs. 4(c) and 4(d) were consistent with those observed for subject A in both pre-RT and post-RT. These results demonstrate that the average landmark registration error is on the order of 1 mm for both subjects.

III.B. Regional pulmonary function change and planned radiation dose distribution

Figure 5 illustrates the difference between SICLE method and ELASTIX-NRP method. The first row of the figure shows transverse slices from the target image FB_{PRE} and the template image EE_{POST} at approximately the same anatomic lo-

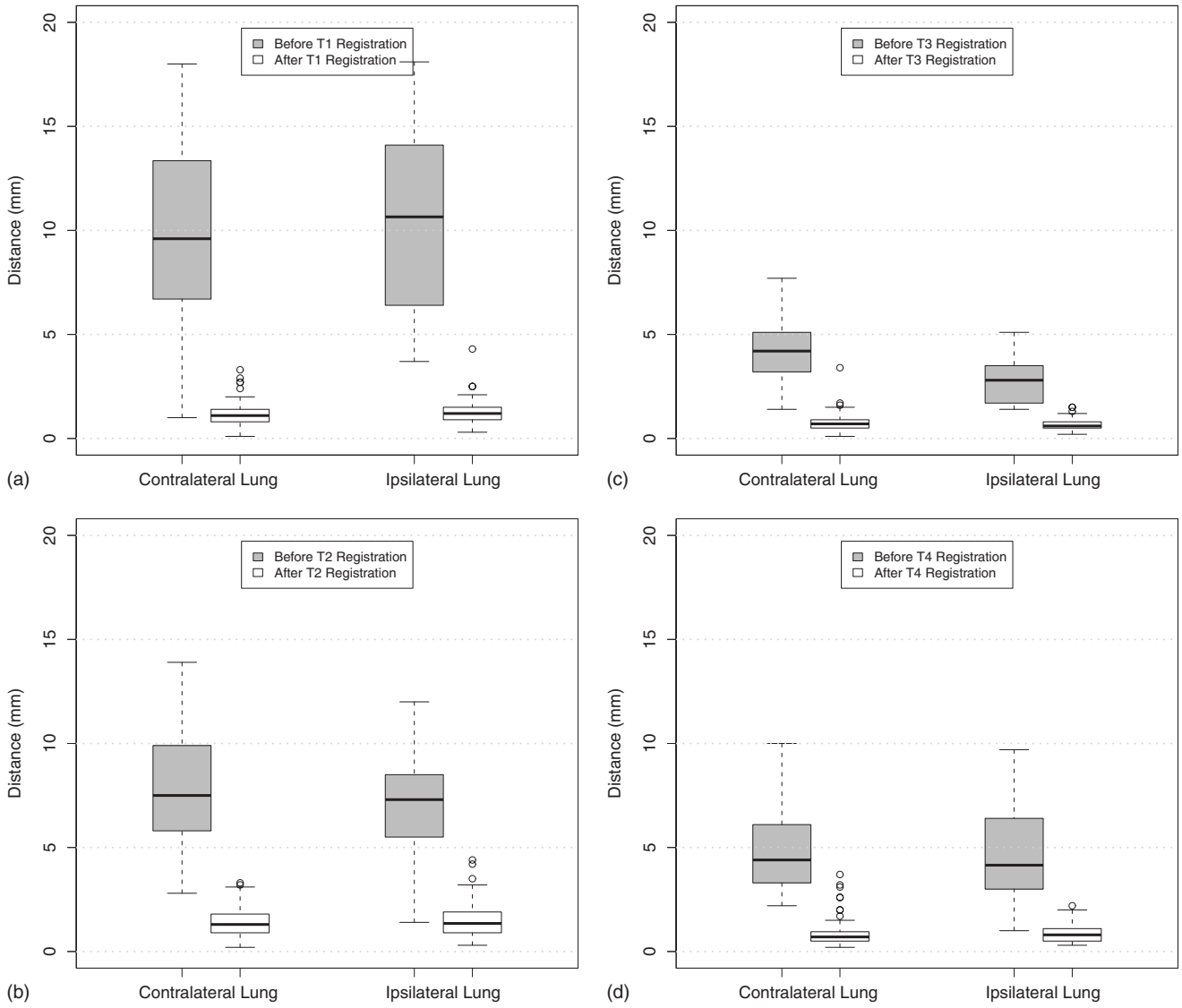

FIG. 4. Landmark distances for subject B before and after registration. Distances between registration pairs (a) T1: EI_{PRE} and EE_{PRE}; (b) T2: EI_{POST} and EE_{POST}; (c) T3: EE_{PRE} and FB_{PRE}; and (d) T4: EE_{POST} and FB_{PRE}. Box plot lower extreme is first quartile; box plot upper extreme is third quartile. Median is shown with solid horizontal line. Whiskers show either the minimum (maximum) value or extend 1.5 times the first to third quartile range beyond the lower (upper) extreme of the box, whichever is smaller (larger). Outliers are marked with circles.

cation. The figure shows that, as expected, the tumor volume has decreased after the RT. The first two figures in the second row show the difference between the registration result (the transformed template image) and the target image for both registration algorithms. While most regions show similar patterns in the difference images, there are some differences in the tissue regions immediately adjacent to the tumor location. Because the SICLE algorithm has no information about the physical properties of tumor region, it forces the tumor boundary to match before and after RT. However, the rigidity map in the ELASTIX-NRP method keeps the tumor as a rigid structure and captures the differences in the tumor region before and after RT. The final figure in the second row shows the difference in pulmonary function change, calculated using SICLE and ELASTIX-NRP to find the T4 transformation. This result shows that there is a difference in the pulmonary function change estimates derived from these two methods in the regions at the upper left and lower left corners of the image around the tumor. Therefore, while SICLE obscures the pulmonary function change in the tumor region because of the lack of information about the physical properties of tumor, ELASTIX-NRP can track the pulmonary function change in the tumor region with local rigidity constraint.

Figure 6 shows the color-coded pulmonary function images and function change image DIFF for both subjects. The first column shows the pulmonary function map before RT. The second column shows the pulmonary function map after RT. Note that the color scales for these images are different for the different subjects because of differences in tidal volume. For example, in subject A, green and blue indicate normally functioning (expanding) lung tissue with a Jacobian value greater than 1.1, while orange and red regions show decreased lung function with a Jacobian value less than 0.95. As described in Section II G, both function images are

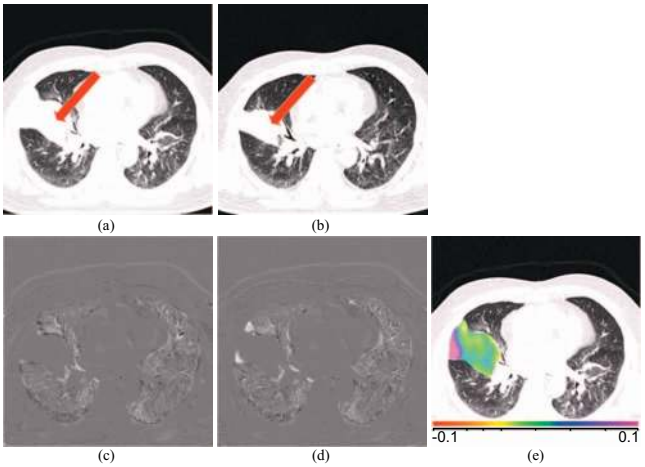

FIG. 5. [(a) and (b)] Target image FB_{PRE} and template image EE_{POST} with red arrows showing the tumor region. [(c) and (d)] Difference of the registration result with the target image for the purely nonrigid registration SICLE and nonrigid registration with local rigidity penalty term ELASTIX-NRP. (e) The difference of the pulmonary function change from SICLE and ELASTIX-NRP.

mapped to FB_{PRE} using transformations T3 and T4. The pulmonary function change images are shown in column three. In the difference images, blue regions represent increased pulmonary function and the red regions represent decreased pulmonary function. The rightmost column in the figure is the planned radiation dose distribution, in units of Grays (Gy). The spatial map of functional changes in column three can be visually compared to the regions receiving the highest radiation doses (column four).

For subject A, the most dramatic change in pulmonary function is seen in the treated left lung (right side of figure), demonstrating changes from significant expansion (green and blue) before RT to little or no expansion (orange to red) after RT in high dose regions. Notice that more regions in the left lung have increased lung function (blue) following RT than the right lung. However, the right lung (left side of the figure) also shows modest changes in lung function while receiving modest radiation (<8 Gy). The Jacobian change ranges from -0.15 to 0.1 with a mean value of -0.02 in the right lung, and from -0.22 to 0.23 with a mean value of -0.02 in the left lung. It is consistent with our expectation that the left lung (ipsilateral lung, where the radiation dose is targeted) has larger change in pulmonary function than the right lung (contralateral lung, where the radiation dose is much lower). The similar mean value of Jacobian change in both lungs may be caused by the small volume of the tumor in subject A. For subject B, the first and second columns show modest changes in pulmonary function before and after RT for the untreated left lung, while there is a large increase in pulmonary function in the treated right lung following 13 of 37 fractions of RT. The third column in subject B also indicates that the rim of the tumor shows an increase in lung function induced by the decrease in tumor volume. The Jacobian change ranges from -0.40 to 0.39 with a mean value of -0.03 in the contralateral lung, and from -0.25 to 0.50 with a mean value of 0.11 in the ipsilateral lung. This change in function might have been concealed if purely nonrigid image registration algorithms were used to estimate T4. The correlation coefficients (linear regression) for pulmonary function change and the radiation dose were calculated for each patient and each lung. For the subject A, the r value is -0.19 in the ipsilateral lung and -0.14 in the contralateral lung. For subject B, the r value is -0.37 in the ipsilateral lung and 0.25 in the contralateral lung. Therefore, the correlation between the pulmonary function change and radiation dose for the whole lung is very weak and other factors such as treatment location may play a role in this relationship.

Figure 7 presents data showing how the relationship between radiation dose and pulmonary function change may have a location-dependent factor. Figures 7(a) and 7(b) show scatter plots of voxel-by-voxel pulmonary function change (Jacobian change) vs radiation dose for the entire contralateral and ipsilateral lung in subject A. Figure 7(a) shows modest increases in pulmonary function in the contralateral lung post-RT, even though there is much less radiation dose in these regions compared to the treated lung. Figure 7(b) shows the same relationship for the ipsilateral lung, where changes in function and radiation doses are much more pronounced. In both lungs, for regions receiving radiation dose smaller than 24 Gy, either an increase or a decrease in pulmonary function is observed. For regions receiving a radiation dose larger than 24 Gy, all regions show a decrease in pulmonary function.

Figures 7(c)–7(f) show scatter plots between pulmonary function change and radiation dose in the ipsilateral lung within disk-shaped regions at fixed distances from the tumor center. A weak correlation between the dose and pulmonary function change is found at distances from 20 to 25 mm to the tumor (linear regression, $r=-0.73$), suggesting that detected locally compromised pulmonary function may have resulted from radiation injury. The figures shown for other distances from the tumor center do not portray such a simple linear relationship. It is likely that dose and distance from the tumor are not the only factors affecting pulmonary function change, and factors such as the initial pulmonary function within the region, anatomic location, and proximity to other pulmonary anatomy will have an effect. More work is needed to investigate these effects and their complex interrelationships.

IV. CONCLUSIONS and DISCUSSION

We have described a method to measure radiation induced spatial pulmonary function change using 4DCT and image registration. Major vascular bifurcations are used as landmarks to evaluate the image registration. Average registration landmark error is on the order of 1 mm.

The SICLE algorithm is used to assess local lung expansion via the Jacobian of the image registration transformation. The SICLE and ELASTIX-NRP registration methods are used to transform the Jacobian images into the same coordinate system for comparison, and for comparison with the radiation dose map.

The ELASTIX-NRP algorithm was used with a local rigid-

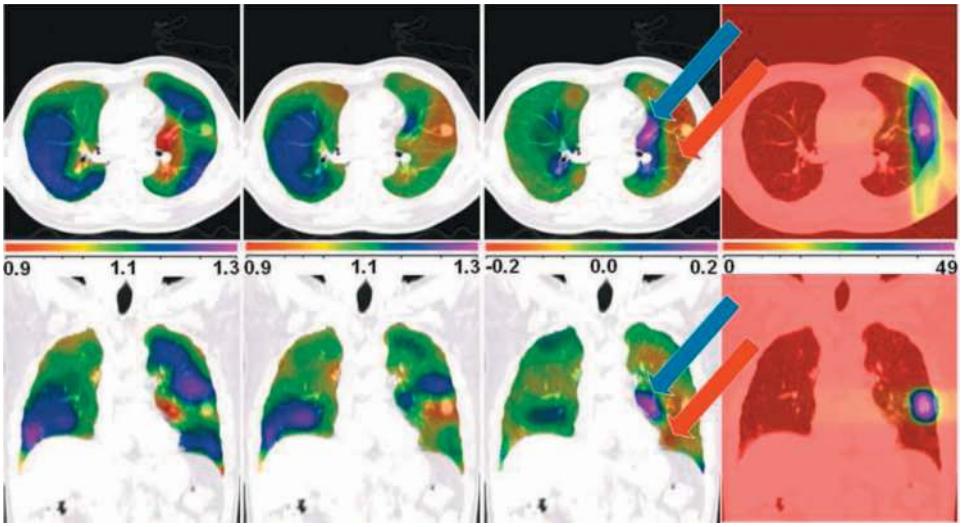

(a) Subject A

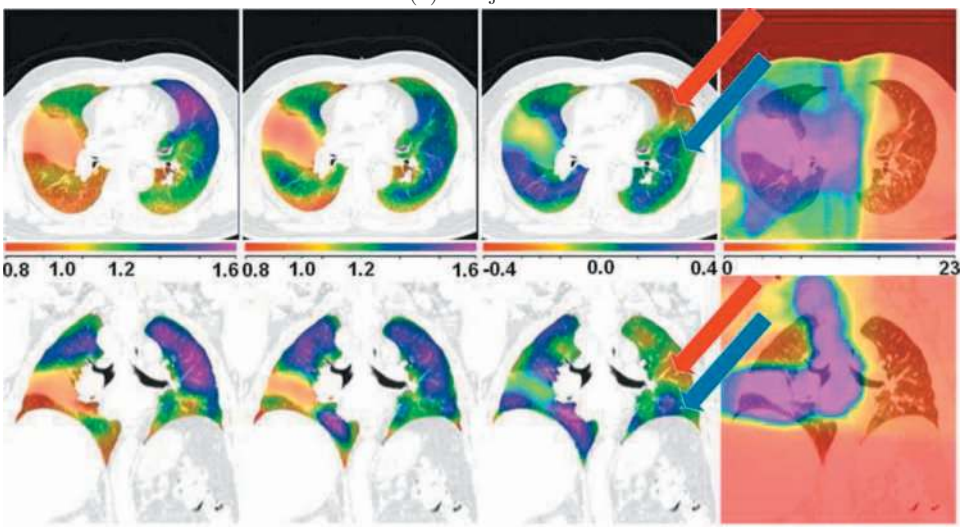

(b) Subject B

FIG. 6. The pulmonary function change compared to the planned radiation dose distribution. The dose map, pulmonary function, and pulmonary function change are overlaid on the FB_{PRE}. The first column is the pulmonary function before RT. The second column is the pulmonary function after RT. The third column is the pulmonary function change from the subtraction of the previous two images. The fourth column is the planned radiation dose distribution. In the third column, the red arrows show regions with decreased pulmonary function, and the blue arrows show regions with increased pulmonary function.

ity map to account for the change in lung tumor size before and after RT. Using this approach, the increased pulmonary function of the regions outside tumor after RT can be mapped correctly to the regions inside tumor before RT. For simplicity, we set the rigidity coefficient for the tumor region in the EE_{POST} as 1 (0 as completely nonrigid tissue and 1 for rigid tissue). However, in the EE_{PRE} to FB_{PRE} registration using the inverse consistent registration, the average Jacobian value in the tumor region is about 0.94, which indicates that there is a small amount of compression in the tumor region (a value of unity indicates no expansion or contraction). Therefore, more experimentation is needed to find the best rigidity coefficient in tumor to yield physiologically meaningful results.

The pulmonary function change measured by change in the Jacobian of the image registration transformations was compared to the planned radiation dose distribution in two subjects. One subject had fully completed the entire course of RT and the other subject had completed about one third of the treatment (13 of 37 fractions).

In this study, the difference in pulmonary function change between the treated lung and nontreated lung was examined within each subject. Since in both patients the tumor was confined to one lung (left lung for subject A and right lung for subject B), the pulmonary function change observed in the contralateral lung may be able to serve as a control for the changes observed in the ipsilateral lung. Caution should be used with this approach since spatial functional changes appear to be a function of more than planned radiation dose. Figure 6 shows noticeable differences in pulmonary function change between the untreated regions and the treated regions. These differences correlate well with the radiation dose distribution in the high dose regions. Therefore, a more

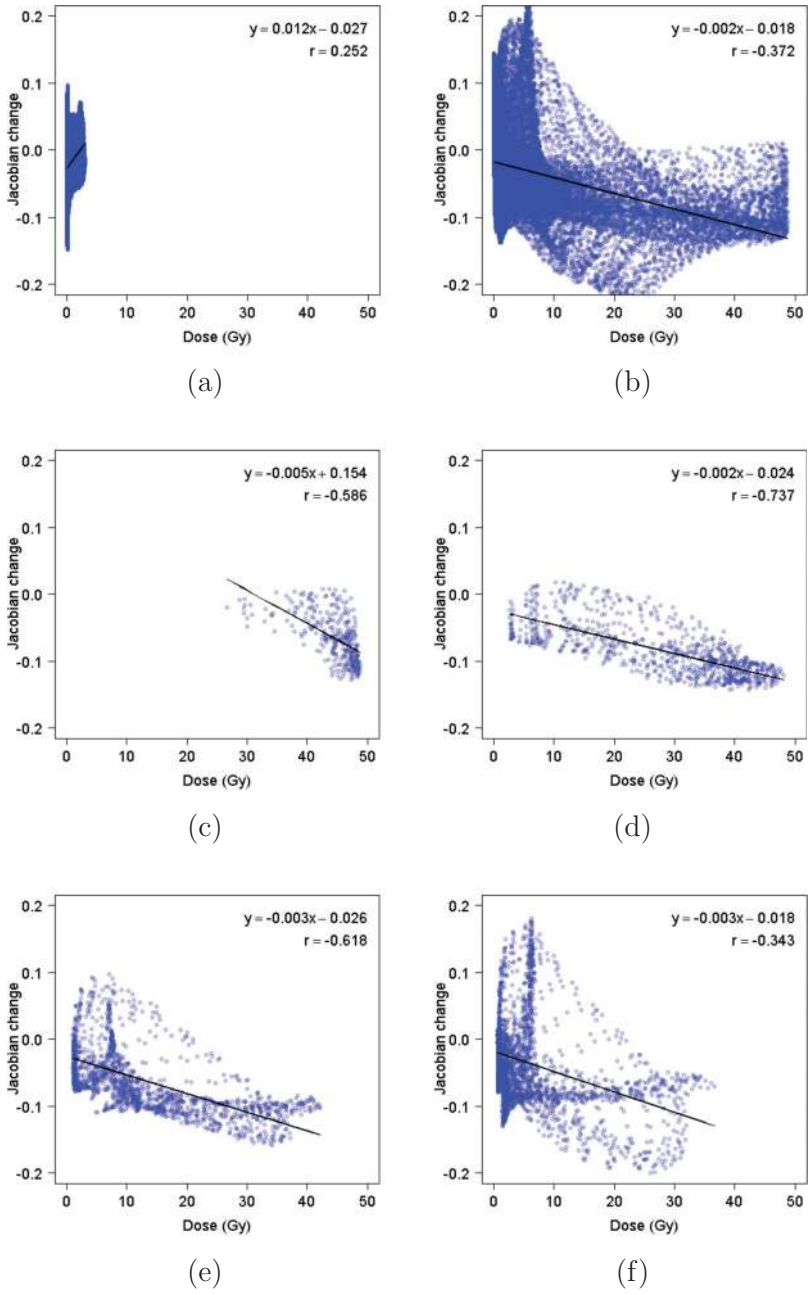

FIG. 7. Pulmonary function change in subject A compared to the radiation dose in scatter plot with linear regression in (a) contralateral lung, (b) ipsilateral lung, and in the ipsilateral lung regions which are at the distance of (c) 10–15, (d) 20–25, (e) 30–35, and (f) 40–45 mm to the center of tumor region.

sophisticated analysis that divides the region based on the isocontours of the radiation dose may be more effective in describing this relationship.

In subject A, the treated regions show a large decrease in pulmonary function (red) around tumor region and a large increase in pulmonary function (blue) in the ipsilateral lung. For subject B, there is a significant increase in the pulmonary function at the basal regions of the treated (right) lung after the treatment indicating the effectiveness of the radiation therapy. Since the EE_{POST} and EI_{POST} images for subject B are acquired after one third of the RT treatments, it would be interesting to acquire additional EE_{POST} and EI_{POST} images at other points during therapy so that pulmonary function change can be examined throughout the treatment.

The results in Fig. 7 show that function change is not only a function of dose, but that there is likely a spatial dependence between the dose distribution and pulmonary function change as well. Other factors, such as initial level of pulmonary function, anatomic location and proximity to the surrounding anatomy, and the effects of a particular RT treatment plan, may also impact lung tissue function change post-RT. Additional work, perhaps using animal models, is required to investigate these effects and their complex interrelationships.

One uncertainty of this comparison is introduced by the difference between the planned and actual dose. The delivered dose at each voxel could be estimated by convolving the planned dose with the known respiratory motion. The motion

used would need to be unique for each fraction delivered. Our approach assumes insignificant lung tissue motion to occur during radiation delivery, as the treatment delivery was gated to allow respiratory motion less than the resolution of the dose grid.

The analysis has been limited to comparing response in the ipsilateral vs contralateral lung. However, it would be natural to consider changes in pulmonary function at the lobar level as well. It is our expectation that regional pulmonary function may also be affected mechanically by the neighboring lobe. Lobar segmentations, such as those provided by Ref. 42, could be overlaid on top of both the dose distribution maps and the pulmonary function change images to observe these effects on a lobe-by-lobe basis.

In conclusion, we have described a method to measure regional pulmonary function change following a course of radiation therapy using image registration. This method may be useful to study the relationships between radiation dose distribution and pulmonary function change, to increase our understanding of the lung toxicity, and to improve radiation therapy for lung tumor control.

ACKNOWLEDGMENTS

The authors would like to thank Ms. K. Murphy and Dr. B. van Ginneken for providing the software IX for annotating landmarks, and Dr. M. Staring for his valuable advice concerning the nonrigid registration with local rigidity. This work was supported in part by NIH Grant Nos. HL079406 and EB004126. This work benefited from the use of ELASTIX, software developed by Dr. S. Klein and Dr. M. Staring, originally developed at the Image Sciences Institute (ISI), on funding granted by the Netherlands Organization for Scientific Research (NWO). ELASTIX is available at http://elastix.isi.uu.nl.

[a]Author to whom correspondence should be addressed. Electronic mail: joe-reinhardt@uiowa.edu; Telephone: (319) 335-5634; Fax: (319) 335-5631.

[1]F.-M. Kong, R. K. T. Haken, M. J. Schipper, M. A. Sullivan, M. Chen, C. Lopez, G. P. Kalemkerian, and J. A. Hayman, "High-dose radiation improved local tumor control and overall survival in patients with inoperable/unresectable non-small-cell lung cancer: Long-term results of a radiation dose escalation study," Int. J. Radiat. Oncol., Biol., Phys. **63**(2), 324–333 (2005).

[2]J. Y. Chang, P. A. Balter, L. Dong, Q. Yang, Z. Liao, M. Jeter, M. K. Bucci, M. F. McAleer, R. J. Mehran, J. A. Roth, and R. Komaki, "Stereotactic body radiation therapy in centrally and superiorly located stage I or isolated recurrent non-small-cell lung cancer," Int. J. Radiat. Oncol., Biol., Phys. **72**(4), 967–971 (2008).

[3]R. Onimaru, M. Fujino, K. Yamazaki, Y. Onodera, H. Taguchi, N. Katoh, F. Hommura, S. Oizumi, M. Nishimura, and H. Shirato, "Steep dose-response relationship for stage I non-small-cell lung cancer using hypofractionated high-dose irradiation by real-time tumor-tracking radiotherapy," Int. J. Radiat. Oncol., Biol., Phys. **70**(2), 374–381 (2008).

[4]R. McCammon, T. E. Schefter, L. E. Gaspar, R. Zaemisch, D. Gravdahl, and B. Kavanagh, "Observation of a dose-control relationship for lung and liver tumors after stereotactic body radiation therapy," Int. J. Radiat. Oncol., Biol., Phys. **73**(1), 112–118 (2009).

[5]T. Xia, H. Li, Q. Sun, Y. Wang, N. Fan, Y. Yu, P. Li, and J. Y. Chang, "Promising clinical outcome of stereotactic body radiation therapy for patients with inoperable stage I/II non-small-cell lung cancer," Int. J. Radiat. Oncol., Biol., Phys. **66**(1), 117–125 (2006).

[6]M. V. Graham, J. A. Purdy, B. Emami, W. Harms, W. Bosch, M. A. Lockett, and C. A. Perez, "Clinical dose-volume histogram analysis for pneumonitis after 3D treatment for non-small cell lung cancer (NSCLC)," Int. J. Radiat. Oncol., Biol., Phys. **45**(2), 323–329 (1999).

[7]G. Paiman, L. B. Marks, Z. Vujaskovic, and C. R. Kelsey, "Radiation-induced lung injury. Assessment, management, and prevention," Oncology (Williston Park, NY) **22**(1), 37–47 (2008).

[8]M. L. Hernando, L. B. Marks, G. C. Bentel, S.-M. Zhou, D. Hollis, S. K. Das, M. Fan, M. T. Munley, T. D. Shafman, M. S. Anscher, and P. A. Lind, "Radiation-induced pulmonary toxicity: A dose-volume histogram analysis in 201 patients with lung cancer," Int. J. Radiat. Oncol., Biol., Phys. **51**(3), 650–659 (2001).

[9]S. L. Kwa, J. V. Lebesque, J. C. Theuws, L. B. Marks, M. T. Munley, G. Bentel, D. Oetzel, U. Spahn, M. V. Graham, R. E. Drzymala, J. A. Purdy, A. S. Lichter, M. K. Martel, and R. K. T. Haken, "Radiation pneumonitis as a function of mean lung dose: An analysis of pooled data of 540 patients," Int. J. Radiat. Oncol., Biol., Phys. **42**(1), 1–9 (1998).

[10]P. G. Tsoutsou and M. I. Koukourakis, "Radiation pneumonitis and fibrosis: Mechanisms underlying its pathogenesis and implications for future research," Int. J. Radiat. Oncol., Biol., Phys. **66**(5), 1281–1293 (2006).

[11]Y. Seppenwoolde, J. V. Lebesque, K. de Jaeger, J. A. Belderbos, L. J. Boersma, C. Schilstra, G. T. Henning, J. A. Hayman, M. K. Martel, and R. K. T. Haken, "Comparing different NTCP models that predict the incidence of radiation pneumonitis," Int. J. Radiat. Oncol., Biol., Phys. **55**(3), 724–735 (2003).

[12]V. Mehta, "Radiation pneumonitis and pulmonary fibrosis in non-small-cell lung cancer: Pulmonary function, prediction, and prevention," Int. J. Radiat. Oncol., Biol., Phys. **63**(1), 5–24 (2005).

[13]E. D. Yorke, A. Jackson, K. E. Rosenzweig, S. A. Merrick, D. Gabrys, E. S. Venkatraman, C. M. Burman, S. A. Leibel, and C. C. Ling, "Dose-volume factors contributing to the incidence of radiation pneumonitis in non-small-cell lung cancer patients treated with three-dimensional conformal radiation therapy," Int. J. Radiat. Oncol., Biol., Phys. **54**(2), 329–339 (2002).

[14]O. Chapet, B. A. Fraass, and R. K. T. Haken, "Multiple fields may offer better esophagus sparing without increased probability of lung toxicity in optimized IMRT of lung tumors," Int. J. Radiat. Oncol., Biol., Phys. **65**(1), 255–265 (2006).

[15]B. P. Yaremko, T. M. Guerrero, J. Noyola-Martinez, R. Guerra, D. G. Lege, L. T. Nguyen, P. A. Balter, J. D. Cox, and R. Komaki, "Reduction of normal lung irradiation in locally advanced non-small-cell lung cancer patients, using ventilation images for functional avoidance," Int. J. Radiat. Oncol., Biol., Phys. **68**(2), 562–571 (2007).

[16]S. M. McGuire, S. Zhou, L. B. Marks, M. Dewhirst, F.-F. Yin, and S. K. Das, "A methodology for using SPECT to reduce intensity-modulated radiation therapy (IMRT) dose to functioning lung," Int. J. Radiat. Oncol., Biol., Phys. **66**(5), 1543–1552 (2006).

[17]Q.-S. Ng, V. Goh, J. Milner, A. R. Padhani, M. I. Saunders, and P. J. Hoskin, "Acute tumor vascular effects following fractionated radiotherapy in human lung cancer: In vivo whole tumor assessment using volumetric perfusion computed tomography," Int. J. Radiat. Oncol., Biol., Phys. **67**(2), 417–424 (2007).

[18]P. van Luijk, A. Novakova-Jiresova, H. Faber, M. N. Steneker, H. H. Kampinga, H. Meertens, and R. P. Coppes, "Relation between radiation-induced whole lung functional loss and regional structural changes in partial irradiated rat lung," Int. J. Radiat. Oncol., Biol., Phys. **64**(5), 1495–1502 (2006).

[19]P. van Luijk, H. Faber, H. Meertens, J. M. Schippers, J. A. Langendijk, S. Brandenburg, H. H. Kampinga, and R. P. Coppes, "The impact of heart irradiation on dose-volume effects in the rat lung," Int. J. Radiat. Oncol., Biol., Phys. **69**(2), 552–559 (2007).

[20]A. Novakova-Jiresova, P. van Luijk, H. van Goor, H. H. Kampinga, and R. P. Coppes, "Changes in expression of injury after irradiation of increasing volumes in rat lung," Int. J. Radiat. Oncol., Biol., Phys. **67**(5), 1510–1518 (2007).

[21]V. A. Semenenko, R. C. Molthen, C. Li, N. V. Morrow, R. Li, S. N. Ghosh, M. M. Medhora, and X. A. Li, "Irradiation of varying volumes of rat lung to same mean lung dose: A little to a lot or a lot to a little?," Int. J. Radiat. Oncol., Biol., Phys. **71**(3), 838–847 (2008).

[22]J. G. Venegas, T. Winkler, G. Musch, M. F. V. Melo, D. Layfield, N. Tgavalekos, A. J. Fischman, R. J. Callahan, G. Bellani, and R. S. Harris, "Self-organized patchiness in asthma as a prelude to catastrophic shifts," Nature (London) **434**(2–3), 777–782 (2005).

[23]R. S. Harris and D. P. Schuster, "Visualizing lung function with positron

emission tomography," J. Appl. Physiol. **102**(1), 448–458 (2006).
[24]K. Suga, "Technical and analytical advances in pulmonary ventilation SPECT with xenon-133 gas and Tc-99m-technegas," Ann. Nucl. Med. **16**(5), 303–310 (2002).
[25]H. E. Möller, X. J. Chen, B. Saam, K. D. Hagspiel, G. A. Johnson, T. A. Altes, E. E. de Lange, and H.-U. Kauczor, "MRI of the lungs using hyperpolarized noble gases," Magn. Reson. Med. **47**(6), 1029–1051 (2002).
[26]E. J. van Beek, J. M. Wild, H.-U. Kauczor, W. Schreiber, J. P. Mugler III, and E. E. de Lange, "Functional MRI of the lung using hyperpolarized 3-helium gas," J. Magn. Reson Imaging **20**(4), 540–554 (2004).
[27]E. A. Hoffman and E. van Beek, "Hyperpolarized media MR imaging—Expanding the boundaries?," Acad. Radiol. **13**(8), 929–931 (2006).
[28]C. Marcucci, D. Nyhan, and B. A. Simon, "Distribution of pulmonary ventilation using Xe-enhanced computed tomography in prone and supine dogs," J. Appl. Physiol. **90**(2), 421–430 (2001).
[29]D. Chon, B. A. Simon, K. C. Beck, H. Shikata, O. I. Saba, C. Won, and E. A. Hoffman, "Differences in regional wash-in and wash-out time constants for xenon-CT ventilation studies," Respir. Physiol. Neurobiol. **148**(1–2), 65–83 (2005).
[30]G. E. Christensen, J. H. Song, W. Lu, I. E. Naqa, and D. A. Low, "Tracking lung tissue motion and expansion/compression with inverse consistent image registration and spirometry," Med. Phys. **34**(6), 2155–2163 (2007).
[31]T. Guerrero, K. Sanders, J. Noyola-Martinez, E. Castillo, Y. Zhang, R. Tapia, R. Guerra, Y. Borghero, and R. Komaki, "Quantification of regional ventilation from treatment planning CT," Int. J. Radiat. Oncol., Biol., Phys. **62**(3), 630–634 (2005).
[32]J. M. Reinhardt, K. Ding, K. Cao, G. E. Christensen, E. A. Hoffman, and S. V. Bodas, "Registration-based estimates of local lung tissue expansion compared to xenon CT measures of specific ventilation," in *Information Processing in Medical Imaging*, special issue of Med. Image Anal. **12**(6), 752–763 (2008).
[33]J. Gee, T. Sundaram, I. Hasegawa, H. Uematsu, and H. Hatabu, "Characterization of regional pulmonary mechanics from serial magnetic resonance imaging data1," Acad. Radiol. **10**(10), 1147–1152 (2003).
[34]K. Ding, K. Cao, G. E. Christensen, E. A. Hoffman, and J. M. Reinhardt, "Registration-based regional lung mechanical analysis: Retrospectively reconstructed dynamic imaging versus static breath-hold image acquisition," Proc. SPIE **7262**, 72620D-1–72620D-9 (2009).
[35]G. Christensen and H. Johnson, "Consistent image registration," IEEE Trans. Med. Imaging **20**(7), 568–582 (2001).
[36]M. Staring, S. Klein, and J. P. W. Pluim, "A rigidity penalty term for nonrigid registration," Med. Phys. **34**(11), 4098–4108 (2007).
[37]T. Waldron, J. Bayouth, S. Bhatia, and J. Buatti, "Use of music-based breathing training to stabilize breathing motion in respiration correlated imaging and radiation delivery," Int. J. Radiat. Oncol., Biol., Phys. **72**(1), S659–S659 (2008).
[38]S. Hu, E. A. Hoffman, and J. M. Reinhardt, "Automatic lung segmentation for accurate quantitation of volumetric x-ray CT images," IEEE Trans. Med. Imaging **20**(6), 490–498 (2001).
[39]K. Murphy, B. van Ginneken, J. Pluim, S. Klein, and M. Staring, "Semi-automatic reference standard construction for quantitative evaluation of lung CT registration," in Proceedings of the International Conference on Medical Image Computing and Computer-Assisted Intervention 2008, 2008, Vol. 5242, pp. 1006–1013 (unpublished).
[40]Y. Yin, E. A. Hoffman, and C.-L. Lin, "Mass preserving nonrigid registration of CT lung images using cubic B-spline," Med. Phys. **36**(9), 4213–4222 (2009).
[41]M. K. Fuld, R. B. Easley, O. I. Saba, D. Chon, J. M. Reinhardt, E. A. Hoffman, and B. A. Simon, "CT-measured regional specific volume change reflects regional ventilation in supine sheep," J. Appl. Physiol. **104**(4), 1177–1184 (2008).
[42]S. Ukil and J. M. Reinhardt, "Anatomy-guided lung lobar surface detection in x-ray CT images," IEEE Trans. Med. Imaging **28**, 202–214 (2009).